Colloidal systems with competing interactions: from an arrested repulsive cluster phase to a gel†‡

Juan Carlos Fernandez Toledano,[ab] Francesco Sciortino[a] and Emanuela Zaccarelli*[a]

We report an extensive numerical study of a charged colloidal system with competing short-range depletion attraction and long-range electrostatic repulsion. By analyzing the cluster properties, we identify two distinct regions in the phase diagram: a state composed of stable finite-size clusters, whose relative interactions are dominated by long-range repulsion, and a percolating network. Both states are found to dynamically arrest at low temperatures, providing evidence of the existence of two distinct non-ergodic states in these systems: a Wigner glass of clusters and a gel.

1. Introduction

The origin of low-density non-ergodic states in colloidal systems is a matter of continuous debate and ongoing research.[1–5] Several different mechanisms may concur in the formation of these arrested states, depending on the relative ratio between the thermal and binding energy and on the shape and symmetry of the interaction potential. When particles interact *via* excluded volume plus a spherically symmetric, attractive potential, it has been shown that the formation of a gel structure takes place concurrently with a spinodal decomposition process. Gelation results from an arrested phase separation.[6] A different scenario occurs when colloidal particles have a residual electrostatic charge which builds up an additional long-range repulsion in the effective colloid–colloid interaction. This term is often modeled as a Yukawa potential with Debye screening length ξ to take into account the presence of the solvent and counterions.[7] In apolar solutions or under low salt conditions, when particles are sub-micron sized, ξ can become comparable to the particle dimension. This long-range repulsive term can coexist with a short-range attraction (induced for example *via* depletion interactions), generating a competition between aggregation, driven by the attractive part of the potential, and the stabilizing role of the repulsion, which may ultimately suppress the macroscopic phase separation. Indeed, it has been shown that the addition of a long-range repulsion of moderate strength can shift to larger attraction strengths (or lower temperatures) the phase separation,[8,9] eventually inhibiting it.[10–13] In this case a microphase separation into clusters[14–18] of a preferred cluster size and shape takes place, depending on repulsion parameters.[19] When repulsion is moderately short-ranged, *i.e.* $\xi/\sigma \lesssim 0.5$ with σ being the diameter of the colloidal particle, it was observed both in experiments and in simulations that elongated clusters are formed at low enough temperature T.[20,21] The repulsion between such clusters is relatively weak so that they tend to form at low T quasi-ordered columnar structures.[22,23] At large enough packing fraction, the clusters are found to merge into a percolating network.[20,21] This network of clusters exists at low enough T and undergoes dynamical arrest, so that a gel state can be properly identified.[4]

For cases where the repulsion term is considerably longer-ranged, *i.e.* $\xi/\sigma \gtrsim 1$, simulations at low enough colloidal densities[24] have reported the presence of a Wigner glass of clusters. This corresponds to a disordered state of polydisperse clusters (due to finite T) which do not percolate and are actually arrested due to the long-range repulsion, in analogy with the Wigner glass reported by Chaikin and coworkers[25,26] for charged colloidal particles under very dilute conditions, stabilized by the Coulomb repulsion. Recently, a comparison between theory and simulations[27] of Yukawa particles has shown that the ideal mode coupling theory (MCT) provides a quite accurate description of the formation of a particle Wigner glass. The MCT predictions for Yukawa particles have also been exploited for interpreting arrest into a Wigner glasses of clusters, in systems with competing interactions.[24,28] Indeed, once clusters are assumed spherical and monodisperse (in size), the effective cluster–cluster interactions can be modeled in terms of a Yukawa potential, with the same screening length as the one acting between single particles but with a renormalized amplitude.[24]

These earlier works call for additional investigations, in order to further question the existence and the stability of a Wigner glass of clusters, as well as a deeper understanding of cluster–cluster interactions. To this end, it is also relevant to mention a recent simulation study[29] where clusters were observed to arrest, at a not-too-low density, by percolation rather than by

[a]Dipartimento di Fisica and CNR-INFM-SOFT, Università di Roma La Sapienza, P.le A. Moro 2, 00185 Roma, Italy. E-mail: emanuela.zaccarelli@phys.uniroma1.it
[b]Grupo de Física de Fluidos y Biocoloides, Departamento de Física Aplicada, Facultad de Ciencias, Campus Fuentenueva S/N, 18071 Granada, Spain

† This paper is part of a *Soft Matter* issue highlighting the work of emerging investigators in the soft matter field.
‡ Electronic supplementary information (ESI) available: Movies of the system for $\phi = 0.04$, 0.08, 0.125 and 0.14 at $T = 0.1$, referring to a total simulation time of 1×10^5 steps. The movies are made using available configurations every 5000 steps. Clusters are colored according to the number of particles, so that a change in color correspond to a breaking or branching event between clusters. In the cluster phase region, clusters can be seen to essentially only undergo rotational motion, while a translational one is extremely small. When ϕ increases, *e.g.* for $\phi = 0.125$, some cluster branching events can be observed, soon followed by cluster breaking. Above percolation, the gel network remains essentially frozen and motion is due essentially to vibrations. See DOI: 10.1039/b818169a

repulsion. However, differences in the simulation protocol of this work are present with respect to that used in ref. 24, in particular history of quench and quench rate, as well as a shorter cut-off distance for the long-range repulsion potential. Hence, a more comprehensive study of these models in a wide region of packing fraction ϕ and temperature T, fully accounting for the long range nature of the repulsive interactions, is needed.

In this work we report an extensive simulation study which aims at elucidating in detail the phase diagram of colloidal systems interacting with both short-range attraction and long-range repulsion, encompassing states well below, at the crossing and well above the percolation line at low enough T. We characterize in detail the properties of the aggregates that are formed, both when they exist in finite size objects (clusters) and when they merge into a percolating network. We analyze both particle–particle and cluster–cluster correlations to show that, at low enough packing fractions, the system self-organizes into stable, long-living clusters which do not percolate and do not form ordered structures. The interactions between these clusters can be characterized, for low and intermediate ϕ values, in terms of renormalized long-range repulsive interactions of Yukawa form, as previously hypothesized.[24] Most importantly, despite the high polydispersity and non-sphericity of the clusters, we find that the screening length of cluster–cluster interactions remains unchanged with respect to that of particle–particle interactions, while the repulsion amplitude is found to increase with particle density. At larger ϕ values, when the shape of the clusters starts to significantly deviate from the spherical one and increased packing leads to the arising of branching events, a crossover takes place, ultimately leading to the percolation of the clusters associated to a gel transition. We also monitor the dynamics of the two regions, calling for the existence of two distinct non-ergodic states in this low-density, low-T part of the phase diagram.

2. Description of the simulation protocol and analysis

We consider a system of $N = 1000$ particles of unit mass m interacting with a total pair potential composed of a short-ranged attractive part, modeled for convenience as a generalized Lennard-Jones potential[30] with exponent $\alpha = 100$, and of a long-range screened electrostatic repulsion, modeled as a Yukawa term,

$$V(r) = 4\varepsilon\left[\left(\frac{\sigma}{r}\right)^{2\alpha} - \left(\frac{\sigma}{r}\right)^{\alpha}\right] + A\frac{\exp - r/\xi}{r/\xi} \quad (1)$$

where A is the amplitude of repulsion and ε, the depth of the attractive part, is chosen as the energy unit. Time is measured in units of $\sqrt{m\sigma^2/\varepsilon}$. The choice of $\alpha = 100$, also studied in ref. 19 and 24, ensures a very short-range attraction, corresponding to bond formation only within the first neighbour shell. According to the extended law of corresponding states for spherical short-ranged attractions,[31] the choice of the generalized Lennard-Jones potential is generic for any width and shape of the attractive potential.[6] Note that the cluster ground-state properties have also been shown to be invariant for $\alpha \geq 18$.[19] We fix the parameters of the Yukawa potential to $\xi = 2\sigma$ and $A = 0.2\varepsilon$. For such values a microphase separation into clusters exists.[19,24] To correctly take into account the long-range nature of the interactions we solve the

equations of motion using Ewald summation.[32] Indeed, we have compared results obtained in this way with those based on the use of a finite (although large) cut-off. For our choice of parameters, an underestimate of about 10% for the repulsive potential energy is provided by the use of a finite cutoff at 8ξ, in agreement with previous studies.[33] Hence, despite the significantly increased computational cost, it appears crucial for the case under study to treat the long-range repulsive term with Ewald sum, in order to discriminate cases where clusters truly form a disconnected or a percolating state and to address satisfactorily the nature of the arrested state(s) for the chosen value of ξ.

To model the motion of colloidal particles in a solvent, we use Brownian dynamics simulations with time step $\delta t = 0.005$ and bare diffusion coefficient $D_0 = 0.005$. For this choice, the crossover from ballistic to diffusive regime, for isolated particles, takes place at $t \approx 10$. We do not treat explicitly the effect of the solvent, i.e. hydrodynamic interactions are neglected, but we do not expect these to provide significant changes to the long-time structures that we observe.[34] We neglect any change in the electrostatic parameters, in particular of ξ, with increasing colloid packing fraction ϕ. For particles of the order of μm, this variation is expected not to be significant with respect to the particle diameter.[35]

The system was initially prepared at several densities and high T, and later it was slowly equilibrated to successively lower T. Our aim is to study the approach (from the equilibrium side) to a dynamic arrest transition, rather than a rapid quench inside the region where arrest is observed. We study 9 isochores and several T in the low-ϕ region up to $\phi = 0.20$. Equilibration was carried out in a NVT ensemble, followed by production runs for data collection and analysis. For very low T (depending on the studied ϕ values), a true equilibration is no longer possible. Monitoring for example the energy per particle, the system at first shows a robust decrease towards an apparent equilibrium state, but then the system starts to display a very slow (logarithmic in time) energy drift, typical of an approach to dynamic arrest and trapping in a metastable state.

The connectivity properties of the system have been monitored by studying the interparticle bonding. Two particles are considered bonded when the distance between them is smaller than the position of the local maximum in the interaction potential, i.e. $r < r_b = 1.072\sigma$. When a state point has reached equilibrium, we collect several independent realizations of the system and calculate the distribution $n(s)$ of clusters of size s over time. Moreover, we check whether the largest cluster that we find in the configuration has spanned the whole box at least in one direction. If at least 50% of the considered realizations contains a spanning cluster, the state point is classified as percolating. For state points which do not percolate at the studied T, we monitor the cluster properties in time, finding that the clusters have a finite, but large lifetime. If the cluster size distribution shows a maximum for a finite value of s, indicating that a preferred size for the clusters exists, we classify this state point in the cluster phase region.

3. Finite size clusters and percolation: disordered, metastable states

In Fig. 1 we report the phase diagram of the system in the studied (ϕ,T) region, highlighting the loci of points where (i) a cluster
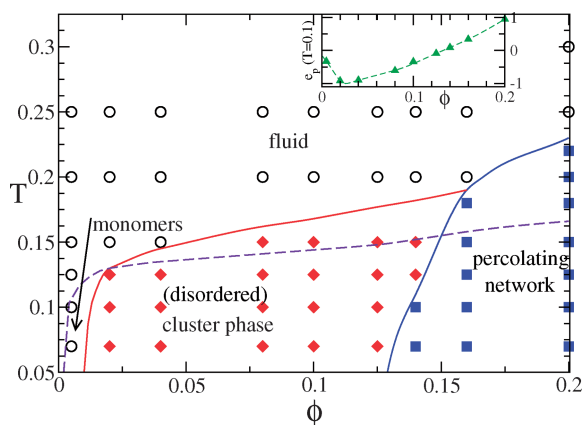
Fig. 1 A phase diagram of the studied system. ○ indicate fluid states (no cluster phase and non-percolating). ◆ indicate points within the cluster phase region [*i.e.* showing a maximum at finite s for $n(s)$] and ■ refer to percolating state-points. The solid line (—) defines the cluster region and the percolation region, and the dashed line (- - -) defines the region (*i.e.* the state points below the line) where the energy starts to display a slow logarithmic drift, drawn as guides to the eye. At a low enough ϕ (*i.e.* $\phi \lesssim 0.02$) the cluster size distribution is peaked at $s = 1$. Inset: potential energy per particle e_p *versus* packing fraction at $T = 0.10$. A minimum is found at very low ϕ values; e_p becomes positive for $\phi > 0.125$, *i.e.* close to the location of the percolation transition.

phase is observed and (ii) the system percolates. We also report a (dashed) line delimiting the region where a true equilibration cannot be reached, meaning that, for all investigated state points below the line, the potential energy keeps displaying a very slow, logarithmic drift for the entire duration of the simulation. This region largely belongs to the portion of the phase diagram where stable clusters and percolation are present.

We notice that in the absence of repulsion, the critical temperature for the short-ranged attractive potential studied here is found at $T_c \simeq 0.24$,[24] while the critical packing fraction is found to be approximately $\phi_c \simeq 0.27$, following the behavior for spherical attractive potentials in the short-range limit.[36] Hence, the addition of a long-range repulsion suppresses the tendency to phase separate macroscopically, at least in the T-window that we have studied, *i.e.* for $T \geq 0.05$. It becomes thus possible to reach lower temperatures in one-phase condition. At these low T, the lifetime of the inter-particle bond increases significantly and clusters behave as effective long-lived aggregates.

Fig. 1 shows that for $\phi \leq 0.125$ the system never percolates at all studied T. For very small ϕ (*e.g.* $\phi = 0.005$) the system organizes into very small clusters, and the maximum of $n(s)$ is located to $s = 1$ at all studied T. We can consider this very low-ϕ region to be essentially in a 'monomeric' state. As the ϕ value is increased, a maximum in the cluster distribution $n(s)$ develops for $T \lesssim 0.15$, and we can identify a stable cluster phase, according to our definition discussed above. In this region, clusters can be monitored in time and we observe that they continuously exchange particles with each other, breaking and reforming bonds, while on average existing at all times in different realizations. For $T \lesssim 0.1$, clusters become more and more long-lived, since the time necessary to break a bond becomes comparable to the simulation time. Similarly, the encounter between two different clusters is quite rare, due to the presence of the long-

range repulsion. Essentially, clusters become frozen. Finally, for $\phi \gtrsim 0.14$ we observe percolating states. Hence, at low T or equivalently for high attraction strengths, the system displays a transition from monomers to a stable finite-cluster phase and eventually to a particle network. These findings are in very good agreement with recent confocal microscopy experiments carried out for a charged colloidal suspension with depletion interactions under low screening conditions,[37] consistent with the case discussed in the present work.

In the inset of Fig. 1, we report the dependence of the potential energy per particle e_p, on ϕ for $T = 0.1$. Data are collected at the end of the long simulation runs (due to the presence of the slow logarithmic aging). We notice that the energy has a minimum at $0.02 < \phi < 0.04$ and then becomes positive for $\phi > 0.125$, *i.e.* in the region where percolation is observed. This points to the fact that particle clustering is dominated by the attractive interactions only at very low ϕ values, while the interplay with repulsion becomes important for $\phi \gtrsim 0.04$. The increase in the energy arises from the large number of neighbours within the repulsive range of the interaction, which overcomes the gain associated to bonding.

To visualize the cluster formation and to highlight the fact that the system at low ϕ values neither percolates, nor forms ordered structures, we report in Fig. 2 some snaphots of the system for different ϕ values along the isotherm $T = 0.10$. Different clusters are drawn in different colors, according to particle number. Although exchange of particles between clusters as well as cluster branching and breaking processes are sometimes observed, a similar picture of clusters to that reported in Fig. 2 exists at all times. The emergence of a percolating cluster arises, for the reported temperature, at $\phi = 0.14$, and rapidly involves the majority of particles as ϕ grows further. We notice that in the cluster phase region, clusters are polydisperse, both in size and in shape. While at low ϕ values they are always rather spherical, they tend to become more and more elongated with increasing packing fraction. This phenomenon was observed in previous simulation[21] and experimental[20] studies for a system with a much shorter screening length. A study of the ground state properties of isolated clusters[19] has shown that, while in the short screening length case quasi one-dimensional cluster growth is energetically favoured, giving rise to the peculiar Bernal spirals,[20,21] for the present study the expected ground state cluster structure is much more spherical, although with some degree of anisotropy. Comparing the ground state structure of clusters of a certain size, shown in Fig. 5 of ref. 19 for the two cases, it is evident that the average number of nearest neighbours is dramatically different: in the Bernal spiral, particles have always exactly 6 neighbours (since there is no difference between bulk and surface), in our case particles in the interior of the cluster have a coordination close to 12 neighbours, while those on the surface a much smaller one (close to 6). Hence, the resulting average coordination is close to 8.

To gain a better understanding of the cluster shape and local structure for the present case, we report in Fig. 3 the (average) distribution of nearest neighbours $P(n)$ for all studied ϕ values for $T = 0.1$, and the average number of neighbours $<n>$ in the associated inset, which is compared to the ground state predictions. While, as expected, the number of nearest neighbours at first increases with ϕ, above percolation it roughly stops evolving, so that $<n>$ does not grow much above 6. Indeed, the
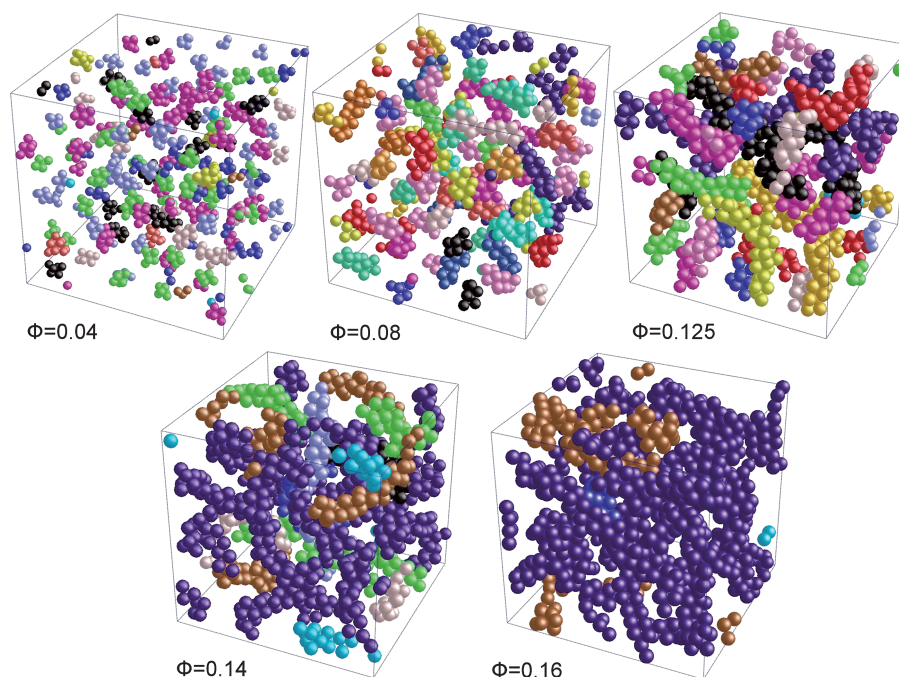
Fig. 2 Snaphots of the simulated system for several different ϕ values at $T = 0.10$. Different clusters are drawn in different colors according to particle number in the cluster. For $\phi \leq 0.125$ (top row), the system forms at all times several distinct clusters which are not connected and do not span the simulation box; while for $\phi \geq 0.14$ (bottom row) a percolating cluster exists at all times.
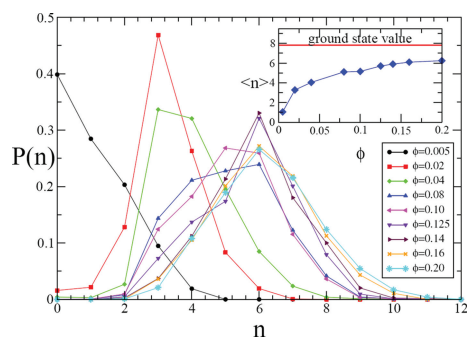

Fig. 3 The distribution of nearest neighbours P(n) for all studied ϕ values and $T = 0.1$. Inset: dependence on ϕ of the average number of neighbours $<n>$ and comparison with isolated clusters ground state predictions from ref. 19.

distribution tends to saturate and to remain always peaked around 6 neighbours, despite a gradual increase in the number of particles with large number of neighbours. Monitoring the evolution of $<n>$ with T (not shown), we do not observe the presence of non-monotonic effects, which were found in the low-screening length case,[21] suggesting that the long-range repulsion never facilitates the formation of compact structures. Comparing with the isolated cluster study of ref. 19, we can argue that the interactions between clusters act against the compaction of the clusters and favor the formation of elongated structures. Indeed, if we imagine cluster–cluster interactions to be ruled by the long-range repulsion (as we will prove below), clusters will occupy the space much more efficiently and, at the same time, reduce the total potential energy due to increased average cluster–cluster distance by growing in an elongated rather than a spherical manner.

Next, we examine the behaviour of the radius of gyration of clusters of size s, defined as $R_g(s) \equiv \dfrac{1}{s^{1/2}} \left\langle \left[\displaystyle\sum_{i=1}^{s} (r_i - R_{CM})^2 \right]^{1/2} \right\rangle$, where r_i is the coordinates of particle i, R_{CM} is the cluster center of mass and the average is performed over all particles of size s. We report $R_g(s)$ in Fig. 4 for all studied ϕ at $T = 0.1$. Percolating clusters are not included in the analysis.

We notice that, in agreement with data in ref. 21, the dependence of R_g on cluster size below the percolation threshold does not show a dependence on ϕ, although larger ϕ values allow sampling of larger cluster sizes. However, as ϕ grows above percolation, clusters gradually become slightly more compact, displaying a smaller R_g at comparable sizes. We can try to
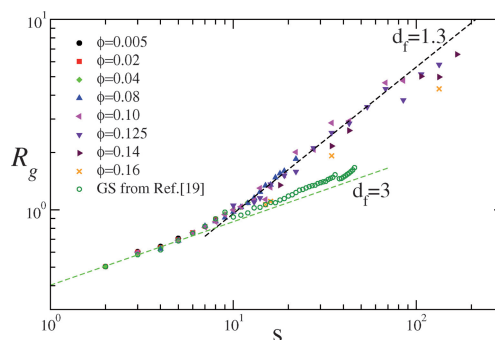

Fig. 4 (a) Radius of gyration of finite-size clusters for all studied ϕ values at $T = 0.1$. Also shown are the ground state calculations (○) for isolated clusters taken from ref. 19. --- indicates power-law behavior s^{1/d_f}, namely spherical ($d_f = 3$) for small sizes and quasi-linear ($d_f = 1.3$) for large sizes.

identify a growth law for R_g with size. For $s \lesssim 10$, clusters are compact objects, as expected. Defining a fractal dimension for clusters d_f as the power law exponent of $R_g \approx s^{1/d_f}$, we find that for $s \gtrsim 10$, clusters lose their compactness and a quasi-linear growth is observed, roughly compatible with an exponent of 1.3. This is close to what is observed for the Bernal spiral case. The figure also shows the corresponding data for the ground state configuration of isolated clusters, taken from ref. 19. In comparison with the isolated clusters' ground states, the clusters observed in the simulations are significantly less compact, suggesting that interactions between clusters and the non-negligible role of entropy already induce a one-dimensional growth at smaller sizes. Hence, the system always remains very far from isolated clusters ground state predictions. This probably results from a combination of effects: on one hand, the increased bond and cluster lifetime does not allow an effective restructuring of the clusters towards their preferred configuration, on the other hand, entropy and cluster–cluster interactions act against spherical growth. In summary, we find the system existing in highly disordered, metastable states, both above and below percolation. This is very clear looking at the movies for several studied ϕ at $T = 0.1$ in the ESI.‡ These results point to the existence of two distinct metastable disordered states, that we are tempted to identify as a Wigner glass of clusters below percolation and a gel state above percolation. To verify whether these two states are kinetically arrested, we examine the dynamics of the system in the following. However, we can already report that an ordered low-T state is never reached during the course of our simulations at any studied ϕ, despite the slow equilibration path that we have used, probably due to the large screening length used. Indeed, a recent study[23] where a much shorter screening length was used (although the potential studied there was not Yukawa-like but exponential) reported the formation of a columnar phase during the course of the simulation: the tendency to order was increased in that case by the reduced repulsive barrier, facilitating formation and breaking of bonds.

Finally, we report the cluster size distribution along the same isotherm, for all studied ϕ, in Fig. 5. We observe a number of relevant phenomena: (i) the emergence of a clear peak between $0.02 \lesssim \phi \lesssim 0.125$, delimiting the cluster phase region for this T as we have defined it and whose boundaries have been represented in Fig. 1. The peak arises at successively larger sizes as
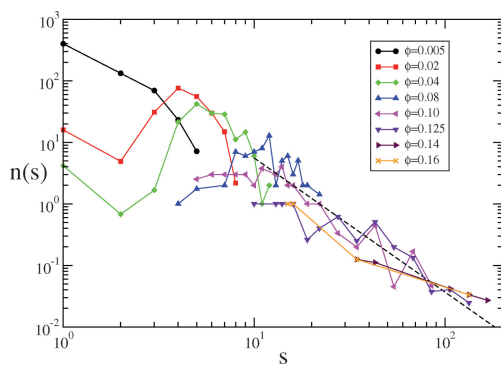
expected; (ii) the gradual disappearance of monomers ($s = 1$), which from being dominant at low ϕ values, in what we have called the monomeric phase, become absent. Not only monomers disappear, but also small clusters of increasing sizes gradually disappear, and the system exists in the form of finite-size clusters; (iii) for increasing ϕ, numerical noise becomes important, due to the small number of finite clusters, but, within such noise, the cluster distribution is consistent with the random percolation power-law prediction, *i.e.* $n(s) \approx s^{-2.2}$.

We conclude this section by observing that, in the present study, we do not find any signature of reentrant percolation as it was found in the short-range repulsion case.[21] In the latter case, at a high enough ϕ, percolation was observed at first for high T, due to random aggregation of particles, then a restructuring into the preferred shape was observed, giving rise to a non-percolating regime for intermediate temperatures, and finally to a new random percolation of the spiral-like clusters at low T. Here, in the investigated region (up to $\phi = 0.20$), we do not observe such behavior.

4. A more careful look at the clusters: intra-cluster and inter-cluster properties

We have seen so far that, at a low ϕ, the system remains organized into several clusters for all studied temperatures. We have also tried deeper quenches (*e.g.* $T = 0.01$), where the system remains far from equilibrium, and we never observe the coalescence of such clusters due to the long-range repulsion. We have also seen that the clusters are polydisperse, even though a preferential size emerges as a peak in the $n(s)$, and that no long-range order is present, *i.e.* we do not observe the presence of any columnar or lamellar phase. However we notice that, at low T, a certain degree of order develops inside the clusters.

By looking at the particle–particle radial distribution function $g(r)$, shown in Fig. 6 for $\phi = 0.08$, clear sharp peaks arise with decreasing T. After a very large maximum at contact (highlighted in the inset), enhanced correlations are found in correspondence of specific discrete distances indicating locally preferred geometries (*e.g.* triangular, tetrahedral, linear order, *etc.*). However,
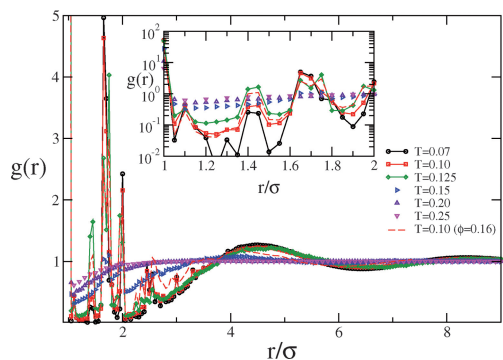

Fig. 5 Cluster size distribution for all studied ϕ values at $T = 0.1$; only non-percolating clusters are included. **---** is the prediction for random percolation $n(s) \approx s^{-2.2}$.

Fig. 6 Radial distribution function $g(r)$ for particle–particle correlations along the isochore $\phi = 0.08$ (within the cluster phase region) and several studied T. Also, results for $\phi = 0.16$ (within the percolating region) at low T (**---**) are reported to show the invariance of the locally preferred positions and liquid-like disorder at large distances in the two connective regimes. Inset: magnification highlighting the contact peak.

liquid-like disorder is retained after the 2nd peak of the $g(r)$. This behaviour is invariant whether we consider states below or above percolation, as also shown in the figure. A parallel analysis of the structure factor (not shown) confirms these observations. This indicates that, at low T, particles inside the clusters tend to occupy preferential ordered positions, thus providing quasi-crystalline character to the inside of the clusters. However, this order is lost already after the second neighbour shell, both in the cluster region and in the percolating one.

After the analysis of particle–particle correlations, it is interesting to consider cluster–cluster correlations to get an idea of what mechanisms regulate the interactions between different clusters and why they do not percolate at sufficiently low ϕ values. In a previous work,[24] it was hypothesized that cluster interactions may be of renormalized Yukawa form, maintaining the same screening length as the underlying particle–particle interactions and with an increased repulsion strength with increasing cluster size. This hypothesis was based on the assumption of spherical and monodisperse clusters, an assumption which is not strictly verified, as we have already discussed, within the present system. To quantify the inter-cluster interactions, we adopt the following strategy. We consider a low enough T where the cluster phase extends over a large ϕ region. In each configuration, for each cluster we calculate its center of mass coordinate. Then, independently of cluster size and shape, we calculate the pair distribution function $g_{CM}^{clust}(r)$ between centers of mass of different clusters. Results for $T = 0.1$ and various studied ϕ are reported in Fig. 7. It is clear that the centers of mass of clusters are found in liquid-like configurations, with increasing correlations as ϕ increases to roughly $\phi = 0.08$. Next we compare the numerical $g_{CM}^{clust}(r)$ with theoretical predictions obtained by solving numerically the Ornstein–Zernike (OZ) equation[7] with the hypernetted chain (HNC) closure. We checked that results are independent of the chosen closure. As suggested in ref. 24, to model the cluster–cluster interaction, we select a pure Yukawa potential (no hard-core), with the same screening length ($\xi = 2.0$) of the particle–particle repulsive interaction. We leave the amplitude A_{eff} of the Yukawa potential as the only fitting
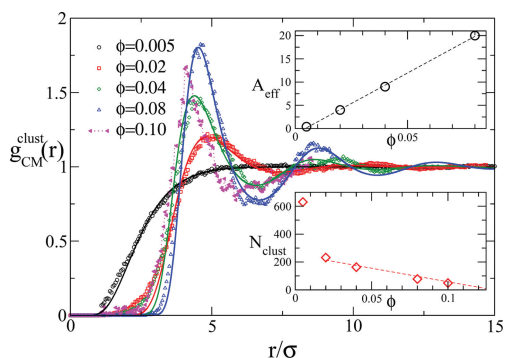
parameter. Indeed, the number density of the clusters is read directly from the simulation data. The best-fit curves are reported in Fig. 7 and show a remarkable agreement with the data extracted from the simulations. The behavior of the cluster number density and of the renormalized amplitude are reported in the insets. A_{eff} grows approximately linearly with ϕ, starting from the particle–particle value at $\phi \to 0$, while the number of clusters progressively shrinks.

Hence, we can describe the system as composed essentially of repulsively-interacting clusters up to $\phi = 0.08$, with a renormalized amplitude which results from the average of all amplitudes which characterize clusters of different sizes and shapes. This result is central for the present paper, and confirms the conjecture put forward in ref. 24, which was then combined with the use of MCT to provide evidence of the existence of a Wigner glass at low ϕ.

The picture of interacting Yukawa clusters breaks for $\phi > 0.08$. The $g_{CM}^{clust}(r)$ can no longer be fitted with a Yukawa analogue. A careful look at the configurations shown in Fig. 2 shows that, at this point, clusters have completely lost their spherical-shape. The radial distribution function shows for $\phi \gtrsim 0.1$ a reversal of trend in the main peak position and amplitude, which then persists at larger ϕ. Moreover, a small peak develops with increasing ϕ for $1 < r/\sigma < 2$, indicating the occurrence of some cluster branching events. The Yukawa effective interaction naturally ceases to work in this regime, and a competition between repulsion and increased packing, favoring sometimes the formation of intercluster bonds, emerges. This mechanism, which can be considered essentially absent for $\phi \lesssim 0.08$, becomes important in this intermediate regime $0.08 < \phi < 0.14$, and finally dominant above percolation. These results highlight the mechanism by which a crossover between a cluster phase and a percolating state is realized, based on a change between repulsion-dominated clusters to a branching regime of clusters favored by the increased packing.

5. Dynamics: MSD and iso-diffusivity lines

Next, we monitor the dynamics of the system, to find out whether and how we approach dynamic arrest at low T, both in the cluster region and in the percolating one. We start by calculating the particle mean squared displacement (MSD), reporting its behaviour in Fig. 8 for $T = 0.1$ and all studied ϕ. We observe a gradual decrease of the MSD with increasing ϕ. From the time dependence of the MSD one can identify distinct regions. For very short times, one observes ballistic motion, followed by a slowing down at short times, which takes place approximately in correspondence with the length scale of the attractive bond distance, defined as $r_{min}/\sigma = (2^{1/100} - 1) \simeq 0.007$, i.e. when two particles are in the minimum of the potential well. This attractive localization by neighbouring particles is active for roughly a decade, even at small ϕ, in the cluster phase region. It is quite remarkable to find particles rattling inside the narrow bonds for such a long time. For intermediate times, particles are able to escape (on average) from the bond, as signalled by the fact that they overcome the distance corresponding to the maximum bond distance $r_{max}/\sigma = (r_b - 1) \simeq 0.072$. Hence, particles explore their neighbourhoods, and a second slowing down emerges. This occurs on length scales that can exceed a particle diameter, depending on ϕ. These results suggest that the motion of a single
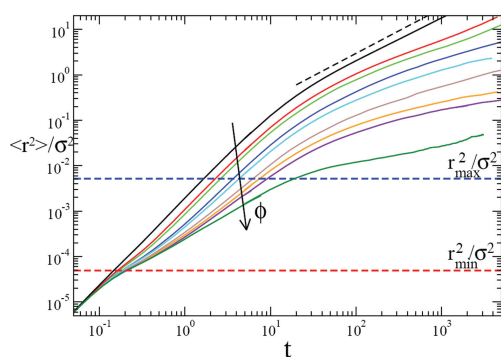
Fig. 7 Radial distribution function between clusters centers of mass for $T = 0.10$ and various studied ϕ in the cluster phase region. Symbols are simulations results, lines are theoretical calculations based on HNC solution of the OZ equation for a renormalized Yukawa interactions. Insets: (a) renormalized amplitude A_{eff} of the Yukawa cluster–cluster interactions and (b) clusters number density (in units of σ^{-3}) dependence on ϕ. --- are linear fits.

Fig. 8 MSD $\langle r^2 \rangle$ *vs.* time for $T = 0.1$ and various ϕ. From top to bottom, $\phi = 0.005, 0.02, 0.04, 0.08, 0.10, 0.125, 0.14, 0.16, 0.20$. **---** indicates diffusive behaviour. Horizontal lines refer to the squared minimum r_{min}^2 and maximum bond distance r_{max}^2 (see text).

particle results from the sum of the Brownian motion of the whole cluster and of the intra-cluster motion. We notice that only the smallest values of ϕ are able to recover a pure diffusive regime at this temperature. For larger ϕ values a sub-diffusive growth of the MSD is found in the time window which can be numerically studied. The apparent exponent regulating the subdiffusivity is found to decrease with ϕ, as expected for an MSD approaching a flat plateau. The onset of subdiffusive behaviour signals that arrest is close-by, and located at slightly lower T, both for the cluster phase region and for the percolating one. In both cases, particles are trapped at first by the attractive bonds with neighbouring particles and secondly by a larger localization length. In the case of a cluster phase, such length provides the distance where clusters can rattle (see movies provided as ESI).‡ For the percolating states, the localization length does not decrease much and the arrested state can be identified as a gel.[4] Interestingly, the transition between the two arrested states is continuous from the MSD point of view.

To further prove that arrest takes place also in the non-percolating regime, we show in Fig. 9 the MSD for $\phi = 0.125$ and various studied T values. We remark that this is an isochore along which the system never percolates, at all studied T, but is the closest, among the studied ϕ values, to the percolation transition. Similar results are found at lower ϕ. At very low T, the

MSD approaches a flat behaviour at long times, so that true arrest occurs. The low-T curves are calculated within a time-window where the energy slowly drifts, and very slow aging effects are thus present. These effects can only slow further the relaxation, so that the reported curves can be considered an overestimation of the true MSDs. The localization length for the arrested state at this ϕ can be estimated around $\sim 0.8\sigma$. The effect of temperature is also visible in the amplitude of the vibration within the bond, which decreases with T, as seen in the height of the inflection around r_{min}.

We note in passing that, in principle, we can also calculate the MSD of clusters (not shown), by monitoring their center of mass trajectory. Due to the fact that clusters undergo breaking and reforming events during the simulation time, statistics are poor. However, in all studied cases, the average MSD of clusters center of mass is always found below that of a single particle. This provides a hint of the fact that, in the explored time window, most of the delocalization is provided by rotational motion of the isolated clusters (see also movies provided in the ESI).‡

From the long-time behaviour of the MSD, we can extract the self-diffusion coefficient, defined as $D = \lim_{t \to \infty} \langle r^2 \rangle / 6t$, for those state points where a diffusive long-time regime can be clearly identified. We can draw iso-diffusivity lines, *i.e.* loci in the phase diagram with constant diffusion coefficient, expressed as a fraction of the bare diffusion coefficient D_0. We plot some iso-diffusivity lines in Fig. 10, together with the phase diagram reported above. We clearly find that the iso-D lines follow the shape of the cluster phase boundary at small ϕ values, while at larger ϕ values they follow the percolation boundary. From previous studies,[38–41] we know that the shape of iso-diffusivity lines does not change much with approaching distance to the $D = 0$ line, which can be identified with the ideal arrest transition. Hence, if one could extrapolate, the arrest line would be somehow parallel to the iso-D lines, signaling that arrest is mainly temperature-driven. Again, we notice the continuous shape of the iso-diffusivity lines across the percolation transition. This allows us to identify low-T states as arrested, or approaching arrest at low T, independently of the presence of a percolating network, the latter condition being discriminant for determining the nature of the two arrested states. Hence, we can conclude that also the non-percolating states undergo dynamical
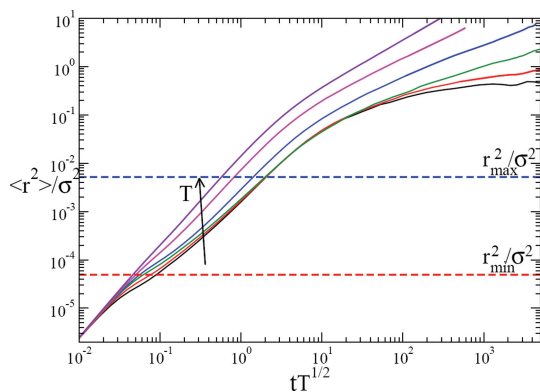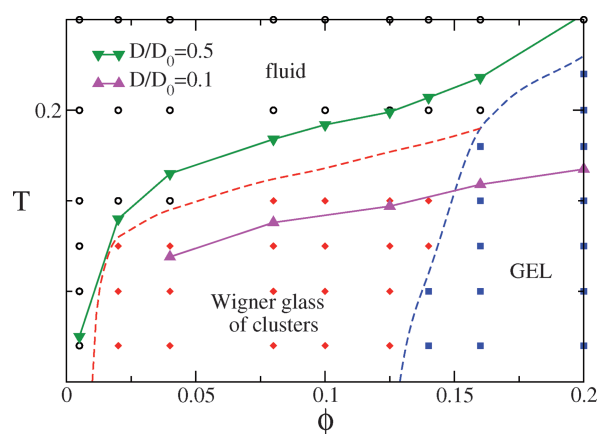

Fig. 9 MSD $\langle r^2 \rangle$ *vs.* time for $\phi = 0.125$ and various T. From top to bottom, $T = 0.2, 0.15, 0.125, 0.10, 0.07, 0.05$. Horizontal lines refer to the squared minimum r_{min}^2 and maximum bond distance r_{max}^2 (see text).

Fig. 10 Phase diagram, partially redrawn from Fig. 1, with added iso-diffusivity lines, for two selected values of D/D_0.

arrest at low T in full analogy with the percolating ones. Thanks to the identification of the dominant cluster–cluster interactions discussed above, arrest at low ϕ can therefore be interpreted as a Wigner glass of clusters, and it is clearly distinct from arrest driven by the formation of a spanning cluster (gel).

Due to the presence of subdiffusion and of aging effects at low T, we can only probe a limited window in D/D_0. The behaviour of D vs. T (not shown) displays a rapid decrease below $T = 0.20$, then followed by a slower (non-Arrhenius) decrease for $T \lesssim 0.125$. Due to the limited available data and the difficulty to extract D for the low-T states, our analysis can not be detailed. However, the apparent non-Arrhenius behaviour might indicate the presence of a finite-T arrest line, at least for the larger densities, and in particular in the gel regime. This is different from what was reported for other gel-forming systems, based on patchy or limited-valence interactions, where Arrhenius behaviour has been observed,[42–44] compatible with an ideal gel state occurring only at $T \rightarrow 0$.[4,45] Indeed, in the patchy particle models, the relaxation and approach to a gel state are essentially controlled by the single-bond lifetime[41] and bonds were shown to be independent. For the present case, the interplay between different types of interactions, and in particular their long-range nature, might be responsible for the fact that collective bond rearrangements are needed in order to restructure the system.

6. Conclusions

In this manuscript, we have reported extensive Brownian dynamics simulations of a model potential suitable to describe the interactions between charged colloidal particles in apolar solvent, in the presence of an additional short-range depletion attraction. The long-range nature of the repulsive screened Coulomb interactions is taken into account numerically by performing Ewald summation. We have studied a wide region of the (ϕ, T) plane, covering the evolution of the system from fluid monomers to a percolating network. In between these two limits, a region of stable finite-size clusters is found. These clusters are spherical at low ϕ, acquiring more and more elongated shape with increasing ϕ, due to the role of cluster–cluster interactions.

We have provided evidence that particles inside clusters can acquire local order, but no long-range order, both inside clusters and among different clusters, is present. Most importantly, we have been able to quantify the cluster–cluster interactions in terms of an effective Yukawa potential, with the same screening length as for particle–particle interactions, and a renormalized amplitude, confirming a previously hypothesized scenario.[24] This happens independently of the clusters' polydispersity in size and shape. However, when ϕ increases, the situation changes, and cluster–cluster interactions become more subtle, due to the increasing number of branching events and to the elongation of the clusters.

At low temperatures, we find evidence of dynamic arrest, by monitoring the MSD and the particles self-diffusion coefficient. The arrest mechanism appears to be continuous across all studied ϕ values and is mostly driven by temperature. However, the distinct nature of the two different low-T states, namely finite-size clusters or a spanning network, allows us to unambiguously identify the presence of two different non-ergodic states in these colloidal systems. A Wigner glass of clusters exists at low/intermediate ϕ values, stabilized by the renormalized Yukawa cluster–cluster interactions discussed above, while a gel state, stabilized by the presence of a percolating, long-lived network takes place at larger ϕ values. It will be interesting in future studies to compute the viscoelastic response of these two different non-ergodic systems, that should manifest extremely different rheological properties. The accurate knowledge of the phase diagram, provided in this work, will allow us to choose the best conditions where such response is measurable and to compare it to those of other gel or glass-forming systems, as well as to experimental results.

References

1 W. C. K. Poon, *Curr. Opin. Colloid Interface Sci.*, 1998, **3**, 593.
2 V. Trappe and P. Sandkühler, *Curr. Opin. Colloid Interface Sci.*, 2004, **8**, 494–500.
3 L. Cipelletti and L. Ramos, *J. Phys.: Condens. Matter*, 2005, **17**, 253.
4 E. Zaccarelli, *J. Phys.: Condens. Matter*, 2007, **19**, 323101.
5 A. M. Puertas and M. Fuchs, *e-print condmat/0810.0681*, 2008.
6 P. J. Lu, E. Zaccarelli, F. Ciulla, A. B. Schofield, F. Sciortino and D. A. Weitz, *Nature*, 2008, **453**, 499.
7 C. N. Likos, *Phys. Rep.*, 2001, **348**, 267–439.
8 D. Pini, J. L. Ge, A. Parola and L. Reatto, *Chem. Phys. Lett.*, 2000, **327**, 209.
9 P. Charbonneau and D. R. Reichman, *Phys. Rev. E*, 2007, **75**, 011507.
10 A. J. Archer and N. B. Wilding, *Phys. Rev. E*, 2007, **76**, 031501.
11 M. Tarzia and A. Coniglio, *Phys. Rev. Lett.*, 2006, **96**, 075702.
12 C. Ortix, J. Lorenzana, M. Beccaria and C. di Castro, *Phys. Rev. B*, 2007, **75**, 195107.
13 C. Ortix, J. Lorenzana and C. di Castro, *Phys. Rev. Lett.*, 2008, **100**, 246402.
14 A. Stradner, H. Sedgwick, F. Cardinaux, W. C. K. Poon, S. U. Egelhaaf and P. Schurtenberger, *Nature*, 2004, **432**, 492–495.
15 A. Imperio and L. Reatto, *J. Phys.: Condens. Matter*, 2004, **16**, 3769.
16 H. Sedgwick, S. U. Egelhaaf and W. C. K. Poon, *J. Phys.: Condens. Matter*, 2004, **16**, 4913.
17 P. Baglioni, E. Fratini, B. Lonetti and S.-H. Chen, *J. Phys.: Condens. Matter*, 2004, **16**, S5003–S5022.
18 F. Cardinaux, A. Stradner, P. Schurtenberger, F. Sciortino and E. Zaccarelli, *Europhys. Lett.*, 2007, **77**, 48804.
19 S. Mossa, F. Sciortino, P. Tartaglia and E. Zaccarelli, *Langmuir*, 2004, **20**, 10756–10763.
20 A. I. Campbell, V. J. Anderson, J. van Duijneveldt and P. Bartlett, *Phys. Rev. Lett.*, 2005, **94**, 208301.
21 F. Sciortino, P. Tartaglia and E. Zaccarelli, *J. Phys. Chem. B*, 2005, **109**, 21942.
22 J. Wu and J. Cao, *Physica A*, 2006, **371**, 249–255.
23 A. de Candia, E. Del Gado, A. Fierro, N. Sator, M. Tarzia and A. Coniglio, *Phys. Rev. E*, 2006, **74**, 010403.
24 F. Sciortino, S. Mossa, E. Zaccarelli and P. Tartaglia, *Phys. Rev. Lett.*, 2004, **93**, 055701.
25 H. M. Lindsay and P. M. Chaikin, *J. Chem. Phys.*, 1982, **76**, 3774–3781.
26 E. B. Sirota, H. D. Ou-Yang, S. K. Sinha, P. M. Chaikin, J. D. Axe and Y. Fujii, *Phys. Rev. Lett.*, 1989, **62**, 1524–1527.

27 E. Zaccarelli, S. Andreev, F. Sciortino and D. R. Reichman, *Phys. Rev. Lett.*, 2008, **100**, 195701.
28 J. Wu, Y. Liu, W.-R. Chen, J. Cao and S. Chen, *Phys. Rev. E*, 2004, **70**, 050401.
29 P. Charbonneau and D. R. Reichman, *Phys. Rev. E*, 2007, **75**, 050401.
30 G. A. Vliegenthart, J. Lodge and H. N. W. Lekkerkerker, *Physica A*, 1999, **263**, 378.
31 M. G. Noro and D. Frenkel, *J. Chem. Phys*, 2000, **113**, 2941–2944.
32 G. Salin and J.-M. Caillol, *J. Chem. Phys.*, 2000, **113**, 10459–10463.
33 A. Giacometti, D. Gazzillo, G. Pastore and T. K. Das, *Phys. Rev. E*, 2005, **71**, 031108.
34 R. Yamamoto, K. Kim, Y. Nakayama, K. Miyazaki and D. R. Reichman, *J. Phys. Soc. Jpn*, 2008, **77**(8), 084804.
35 C. P. Royall, M. E. Leunissen and A. van Blaaderen, *J. Phys.: Condens. Matter*, 2003, **15**, 3581.
36 J. Largo, M. A. Miller and F. Sciortino, *J. Chem. Phys.*, 2008, **128**.
37 Poster presented at the International Soft Matter Conference 2007 by C. L. Klix, C. P. Royall and H. Tanaka.
38 E. Zaccarelli, G. Foffi, K. A. Dawson, S. V. Buldrey, F. Sciortino and P. Tartaglia, *Phys. Rev. E*, 2002, **66**, 041402.
39 G. Foffi, F. Sciortino, P. Tartaglia, E. Zaccarelli, F. Lo Verso, L. Reatto, K. A. Dawson and C. N. Likos, *Phys. Rev. Lett.*, 2003, **90**, 238301.
40 P. Kumar, S. V. Buldyrev, F. Sciortino, E. Zaccarelli and H. E. Stanley, *Phys. Rev. E.*, 2005, **72**, 021501.
41 E. Zaccarelli, I. Saika-Voivod, A. J. Moreno, S. V. Buldyrev, P. Tartaglia and F. Sciortino, *J. Chem. Phys.*, 2006, **124**, 124908.
42 E. Zaccarelli, S. V. Buldyrev, E. La Nave, A. J. Moreno, I. Saika-Voivod, F. Sciortino and P. Tartaglia, *Phys. Rev. Lett.*, 2005, **94**, 218301.
43 E. Bianchi, J. Largo, P. Tartaglia, E. Zaccarelli and F. Sciortino, *Phys. Rev. Lett.*, 2006, **97**, 168301.
44 E. Del Gado and W. Kob, *Phys. Rev. Lett.*, 2007, **98**, 028303.
45 F. Sciortino, S. Buldyrev, C. De Michele, N. Ghofraniha, E. La Nave, A. Moreno, S. Mossa, P. Tartaglia and E. Zaccarelli, *Comp. Phys. Comm.*, 2005, **169**, 166–171.